LA-UR- 04-8195

Approved for public release;
distribution is unlimited.

Title: VERIFICATION AND VALIDATION OF A COMPOSITE MODEL (U)

Author(s): François M. Hemez, Los Alamos National Laboratory, ESA-WR

Trevor B. Tippetts, Los Alamos National Laboratory, ESA-WR

Submitted to: Draft Report of the Los Alamos LDRD-DR "Damage Prognosis" Project, November 2004

VERIFICATION AND VALIDATION OF A COMPOSITE MODEL

François M. Hemez[1], **Trevor B. Tippetts**[2]

Los Alamos National Laboratory
Engineering Sciences and Applications, ESA-WR
Mail Stop T001, Los Alamos, New Mexico 87545, U.S.A.

ABSTRACT

The paper presents preliminary results of applying methods developed for verifying and validating the numerical simulations of multi-layered composite plates. A hierarchy of three validation experiments is defined to validate various aspects of the modeling. The experiments are: modal testing; quasi-static loading; and impact testing. The paper focuses on the validation of the modal response of eight-ply laminated composite plates. After verifying some implementation aspects of the code, mesh convergence studies are conducted. Effect screening is performed to restrict the varying input parameters to the most significant ones. Polynomial meta-models are developed to replace the potentially expensive finite element simulations. Uncertainty is propagated to estimate the variability of predictions given input uncertainty. Test measurements are compared to predictions of modal frequencies. A final statement is made about the predictive accuracy of the composite model and the level of confidence with which modal frequency predictions can be made for potentially different multi-layered configurations. *Approved for unlimited, public release on November 16, 2004, LA-UR-04-8195,* ***Unclassified****.*

1. INTRODUCTION

Multi-scale, non-linear models of composite materials have been developed for several years at the Los Alamos National Laboratory (LANL) in support of various applications such as the LANL Damage Prognosis project. Damage prognosis integrates advanced sensing, data interrogation, statistical pattern recognition, and science-based predictive models to forecast the performance and reliability of engineered systems. Because prognosis relies to a great extent on the deployment of a predictive capability, the credibility of numerical simulations must be established. This is accomplished through various activities collectively referred to as Verification and Validation (V&V).

Results of applying several methods to verify and validate the modeling of multi-layered composite plates are presented [1]. A hierarchy of three validation experiments is defined to validate aspects of the modeling pertinent to the modal, quasi-static, and impact responses [2]. This paper discusses the assessment of prediction accuracy for the modal response of eight-ply laminated composite plates. Mesh convergence errors, parametric variability, and model fitting uncertainty are thoroughly quantified. The predicted natural frequencies are compared to measurements, and a final statement is made about the predictive accuracy of the composite model and its ability to predict potentially different multi-layered configurations.

---

[1] Technical Staff Member and ESA-WR Validation Methods team leader, E-mail: hemez@lanl.gov.

[2] Technical Staff Member of the ESA-WR Materials Behavior team, E-mail: tippetts@lanl.gov.

2. MODAL TESTING OF EIGHT-PLY LAMINATED COMPOSITE PLATES

The modal response of a population of eight nominally identical composite plates is tested. The reason for replicate experiments is to estimate the variability of the modal response due to manufacturing and testing uncertainties. Each plate is 152.0 mm (6.0 inch) square, 1.0 mm (0.04 inch) thick, and made of eight orthotropic carbon fiber plies. Each ply is 0.127 mm (0.005 inch) thick. The ply orientation from top to bottom is a [0; 45; 90; -45; -45; 90; 45; 0] degree combination, which provides symmetry with respect to the mid-layer. In the following, the plies are numbered 1 through 8, from top to bottom. The material properties for the composite material are listed in Section 3. Figure 1 shows the composite plates.

Figure 1. Population of eight-ply composite plates.

The equipment used consists of a laptop computer for data processing and analysis, the Dactron™ data acquisition system, a PCB™ impact hammer, four PCB™ accelerometers, and the corresponding signal conditioners. Each plate is drilled at two adjacent corners and suspended using with a long monofilament, hence, providing free-free boundary conditions. The free-floating boundary is selected because it is the easiest of boundary conditions to simulate numerically.

Data sets are collected using a 4-channel Dactron™ data acquisition system with a bandwidth of 600 Hertz and 4,096 frequency lines. Excitation is provided with a small impact hammer and an exponential window is applied to the measured signals. Three drive point measurements are conducted on each of the eight plates available. Five replicates are collected and averaged for each test to improve the signal-to-noise ratio. Figure 2 illustrates the modal test set-up, and Table 1 lists some of the data acquisition settings.

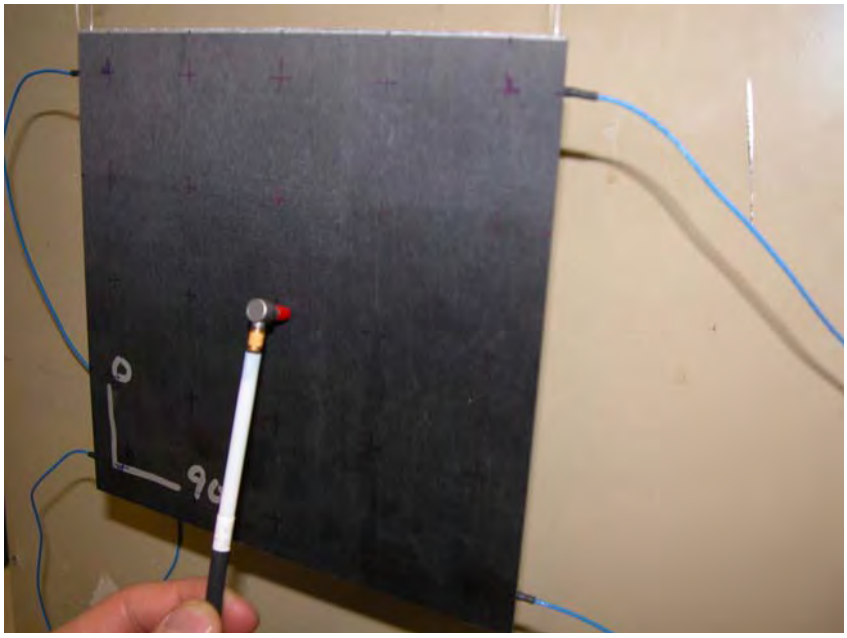

Figure 2. Picture of a suspended composite plate during modal testing.

Table 1. Settings of the data acquisition system.

Channel	Quantity	Engineering Unit (EU)	Input	Sensitivity (m-Volt / EU)	Orientation
1	Force	lbf	1.0	1000.0	-Z
2	Acceleration	g	10.0	10.0	-Z
3	Acceleration	g	10.0	10.0	-Z
4	Acceleration	g	10.0	10.0	-Z

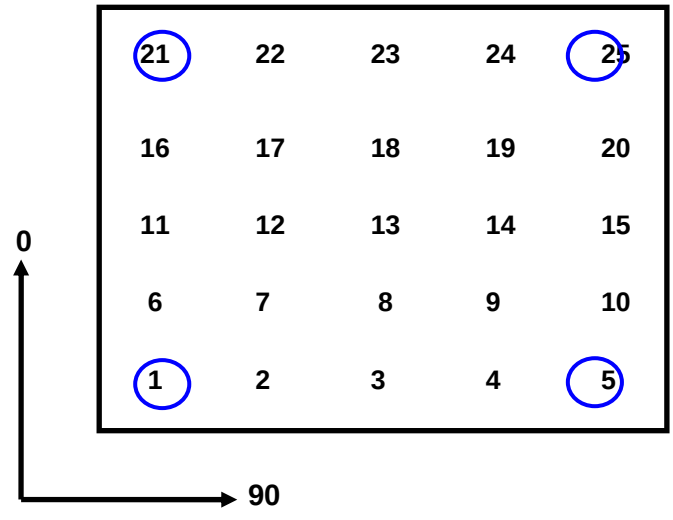

Figure 3. Illustration of accelerometer and impact hammer locations.

Four accelerometers are mounted with wax at the four corners of each plate tested. Figure 3 illustrates the locations 1, 5, 21, and 25 of the four accelerometers (shown with blue circles) relative to the ply orientation angles. The numbers 1-25 shown represent hammer impact locations. Only accelerometers mounted at positions 1, 21, and 25 are connected to the data acquisition system. The fourth accelerometer is placed as a dummy at position 5 to make the instrument loading symmetric and, therefore, emphasize symmetric mode shapes.

For simplicity, the analysis is here restricted to modal frequencies. Mode shape or modal damping predictions of the composite model can be verified and validated using the procedure outlined below. Modal frequencies are preferred because they provide low-dimensional features that well characterize the linear, low-frequency response of the laminate plate.

Tables 2 and 3 show statistics of the first five identified frequencies. Mean and standard deviation values are listed in Table 2. The correlation matrix given in Table 3 is a normalized version of the covariance matrix Σ_{yy}.[3] The covariance matrix Σ_{yy} is estimated by computing:

$$\Sigma_{yy} = \left(Y - \mu_y\right)\left(Y - \mu_y\right)^T \tag{1}$$

where Y denotes the data matrix and μ_y represents the vector of mean frequencies shown in Table 2. The data matrix, Y, collects the frequencies identified for each one of the eight plates:

$$Y = \begin{bmatrix} \omega_{1,1} & \omega_{1,2} & \cdots & \omega_{1,N_M} \\ \omega_{2,1} & \omega_{2,2} & \cdots & \omega_{2,N_M} \\ \vdots & \vdots & \ddots & \vdots \\ \omega_{N_R,1} & \omega_{N_R,2} & \cdots & \omega_{N_R,N_M} \end{bmatrix} \tag{2}$$

where $\omega_{i,j}$ denotes the j^{th} frequency identified ($j=1\ldots N_M$) with the i^{th} composite plate ($i=1\ldots N_R$); the number of modes is $N_M = 5$; and the number of replicates is $N_R = 3 \times 8 = 24$.[4]

Table 2. Statistics of identified modal frequencies.

Mode Number	Mean Frequency	Standard Deviation	Relative Deviation
1	107.37 Hertz	1.05 Hertz	0.98%
2	191.81 Hertz	2.37 Hertz	1.24%
3	274.06 Hertz	2.92 Hertz	1.07%
4	315.31 Hertz	3.13 Hertz	0.99%
5	398.88 Hertz	3.00 Hertz	0.75%

(The relative deviation is the standard deviation divided by the mean, expressed in percent.)

It is concluded from Table 2 that measurements are very repeatable because the standard deviation values of identified frequencies are less than 1¼% of the mean values. Table 3 can be examined to study the correlation between frequency values. Correlation is observed between modes 4 and 5 (85%) and, to a lesser extent, between modes 2 and 3

[3] The covariance matrix is normalized in such a way that entries on its main diagonal are equal to one. To do so, it is pre- and post-multiplied by a diagonal matrix formed with the inverse of the standard deviation values listed in Table 2 for each mode. It results the correlation matrix shown in Table 3.

[4] In reality, more than three drive-point measurements are conducted for some of the eight plates, which explains why more than $N_R = 24$ replicate frequencies are available for correlation analysis.

(62%). Such information is useful, for example, in the context of finite element model updating where parameters are calibrated to improve the agreement between test measurements and model predictions. It suffices to define a fidelity metric from frequencies 1, 2, 4 because the other frequency values are somewhat correlated.

Table 3. Correlation coefficients of identified modal frequencies.

Correlation	Mode 1	Mode 2	Mode 3	Mode 4	Mode 5
Mode 1	100.00%	27.38%	47.27%	14.06%	29.22%
Mode 2	27.38%	100.00%	62.45%	22.63%	37.56%
Mode 3	47.27%	62.45%	100.00%	45.84%	49.57%
Mode 4	14.06%	22.63%	45.84%	100.00%	85.41%
Mode 5	29.22%	37.56%	49.57%	85.41%	100.00%

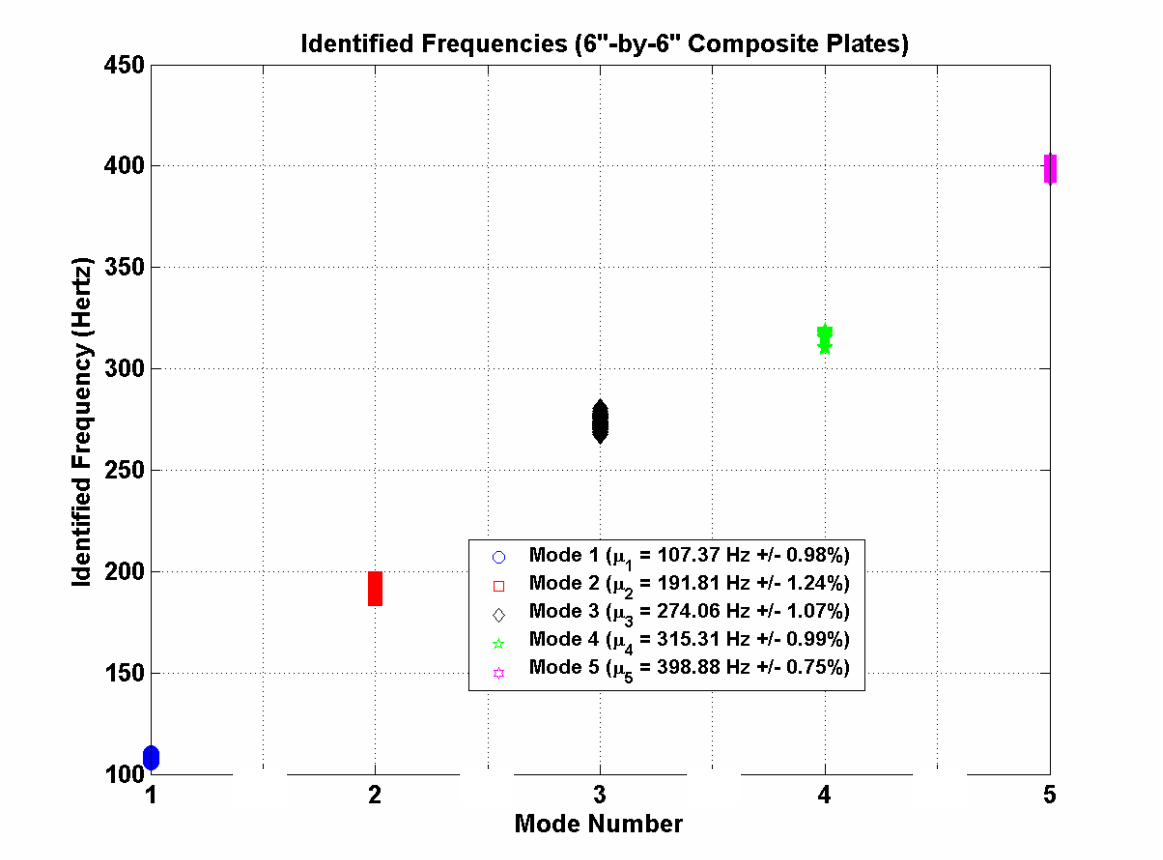

Figure 4. Spread of identified frequencies relative to the low-frequency spectrum.

Figure 4 provides a visual illustration of the frequency variability by showing the small spread relative to the frequency spacing. Figure 5 is similar to Figure 4, except that the mean frequency values are subtracted from each datum to better illustrate the variability. In Figure 5, the symbols represent individual measurements normalized to zero-mean, the solid-line boxes show one standard deviation away from the mean, and the dashed-line boxes show three standard deviations away from the mean. No outlier measurement is observed, which provides

confidence that the manufacturing process of the composite plates was well controlled and little environmental variability polluted the modal measurements.[5]

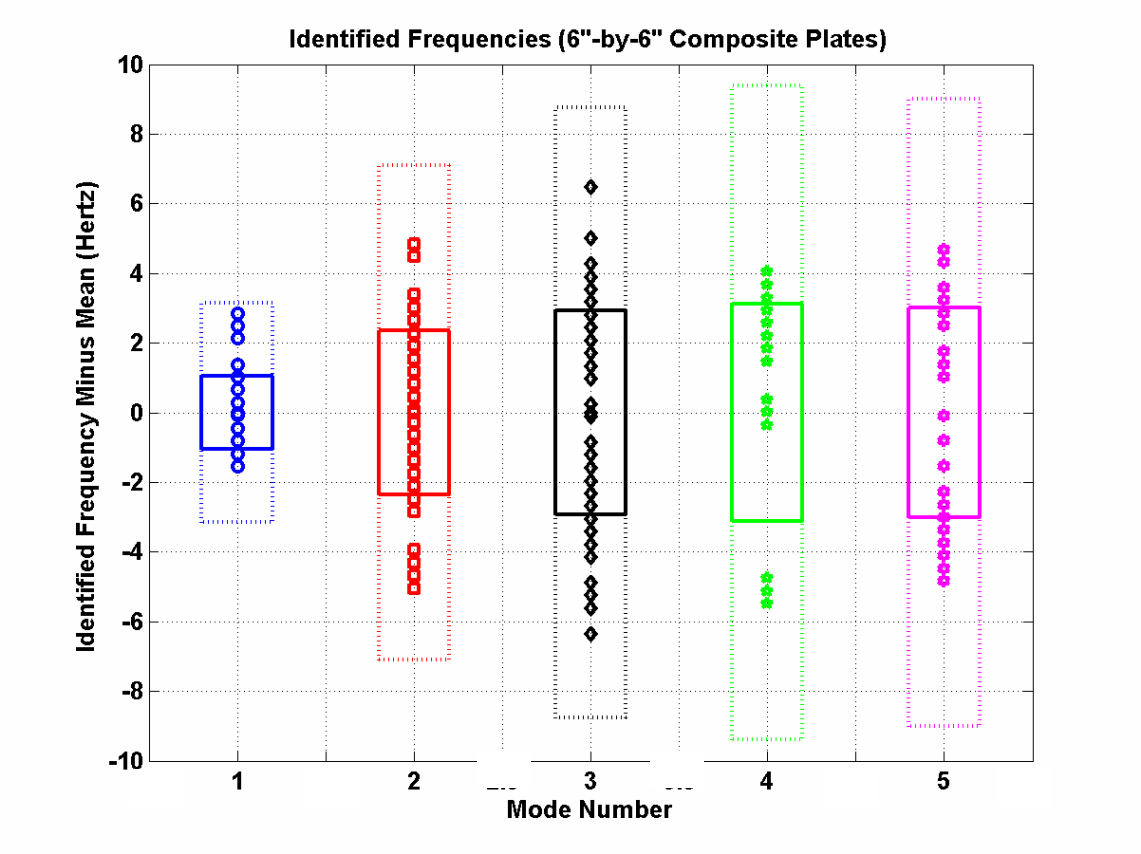

Figure 5. Variability of identified frequencies (mean values removed).

Lastly, the results of a Principal Component Analysis (PCA) are briefly presented. The purpose of this study is to quantify the amount of unit-to-unit variability, that is, the spread of frequency values that may result from what makes the composite plates slightly different from one another. Such factors may include small variations of plate dimensions, lack of material homogeneity, and small differences in the ply alignment. While Figures 4 and 5 quantify the overall variability, plate-to-plate variability cannot be discriminated from test-to-test variability.

The principal components are computed from a Singular Value Decomposition (SVD) of the zero-mean data matrix, that is:

$$\left(Y - \mu_y\right) = U\ \Sigma\ V^T \tag{3}$$

where Σ, U, and V denote the diagonal matrix of singular values, matrix of left singular vectors, and matrix of right singular vectors, respectively. SVD is a computationally efficient calculation of the eigen-vectors of the covariance matrix Σ_{yy}, which is usually how PCA is performed.

[5] An outlier is here defined as a datum that would be more than three standard deviations away from the mean, where the mean and standard deviation values are estimated from the population (see Table 2).

Table 4 lists the singular values of the decomposition. Note that "mode" here refers to a principal component mode, not to be confused with a resonant mode of the structure. The right and left singular vectors are illustrated in Figures 6 and 7, respectively. It can be observed from Table 4 that the first three principal components account for more than 82% of the correlation structure of the data matrix Y. This indicates that the correlation analysis can be restricted to the singular modes 1-3 without loosing too much information.

Table 4. Singular values of the zero-mean modal frequency data matrix.

Singular Mode Number	Singular Value	Percent Contribution
1	39.54	42.66%
2	23.04	24.86%
3	13.54	14.61%
4	9.82	10.60%
5	6.74	7.27%
Total		**100.00%**

(The contribution is the singular value divided by the sum of all singular values, expressed in percent.)

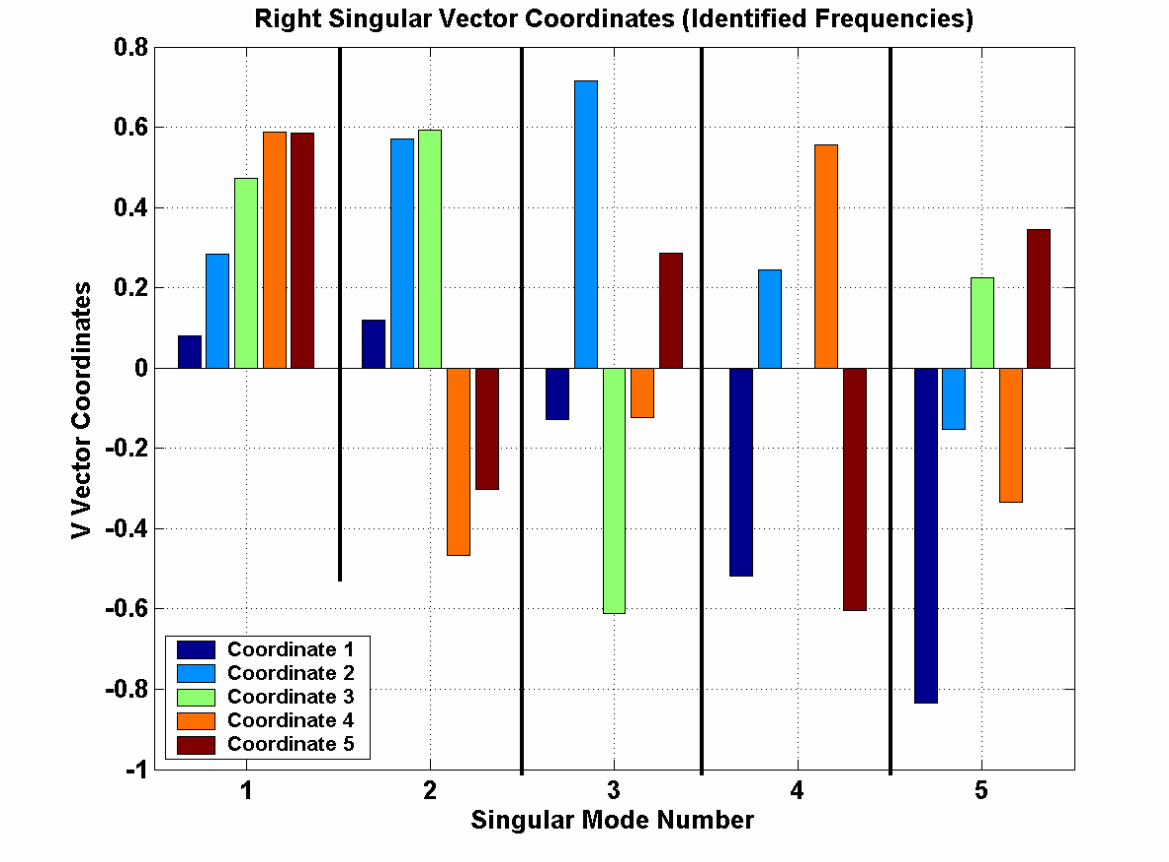

Figure 6. Right singular vectors of the zero-mean modal frequency data matrix.

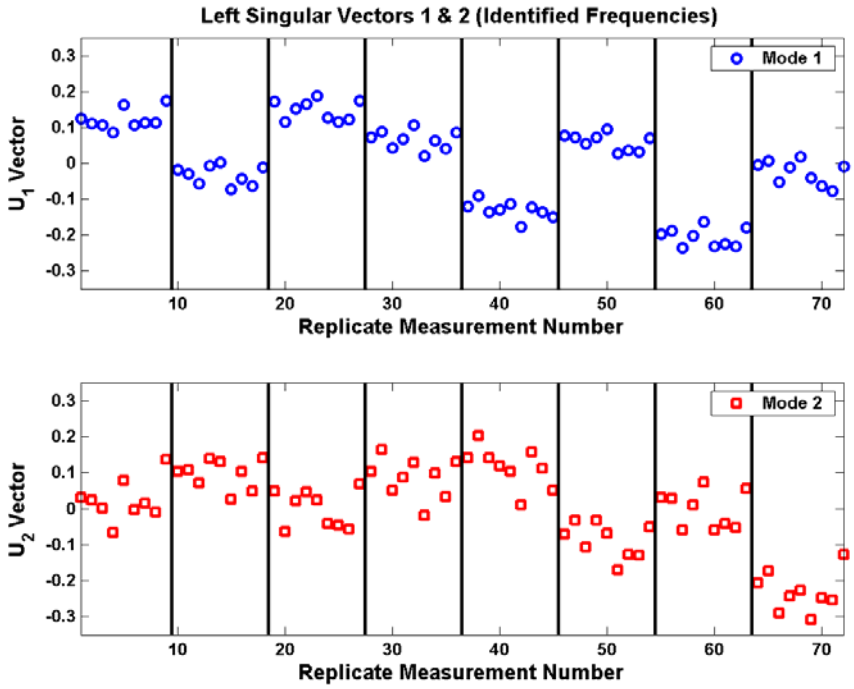

Figure 7 (a). Left singular vectors 1, 2 of the zero-mean modal frequency data matrix.

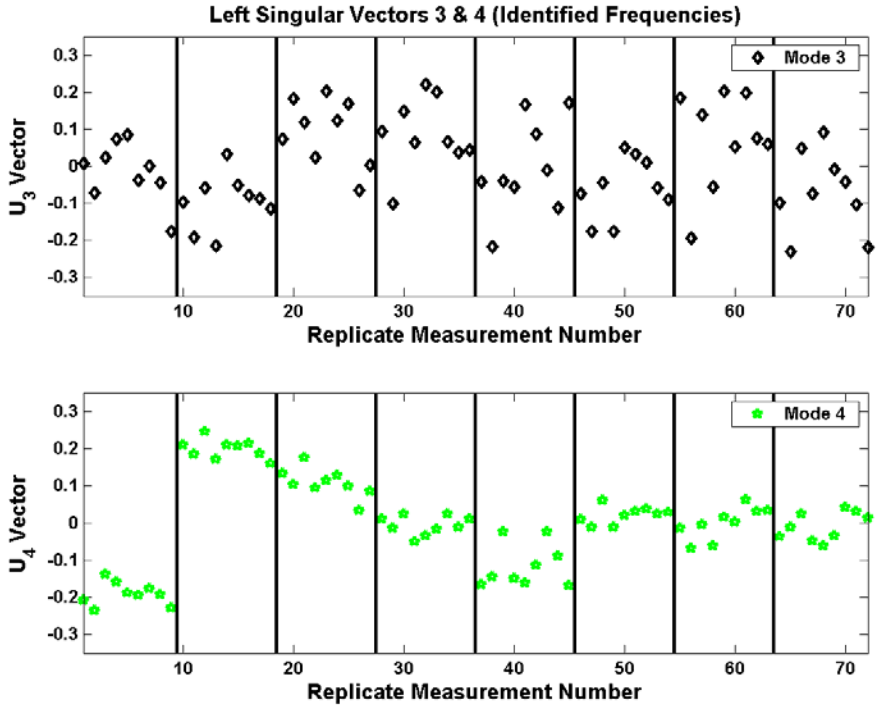

Figure 7 (b). Left singular vectors 3, 4 of the zero-mean modal frequency data matrix.

Figure 6 shows the five right singular vectors, V_k, where each one is a 5-coordinate vector. Modes are separated by solid-line vertical lines. The physical interpretation of right singular vectors is not straightforward. It can be observed, however, that all coordinates of the first right singular vector, V_1, are positive, which indicates a positive trend in the correlation between the first five identified frequencies. This makes sense because an action taken to increase the first natural frequency (such as increasing the elasticity constants) also tends to increase the frequency of higher-order resonant modes. The second right singular vector, V_2, identifies another trend where the correlation between natural frequencies 1-3 and natural frequencies 4-5 is negative. The physical interpretation of the third right singular vector, V_3, is unclear. The relative "strength" of these trends is indicated by their singular values in Table 4.

Figures 7(a) and 7(b) show the left singular vectors, U_k, for principal components 1-2 and 3-4, respectively. The fifth left singular vector, U_5, conveys no interesting information and it is not shown. The length of each U_k vector is equal to the number of replicates, or N_R. Data collected for each plate are separated by solid-line vertical lines which makes it possible to segregate plate-to-plate variability from test-to-test variability. The analysis focuses on the first principal component mode, U_1, for simplicity. It can be observed that the spread of coordinates is somewhat discontinuous when transitioning from one plate to the next. The amplitudes of these "jumps" are larger than the spread observed for the same plate tested. This indicates that plate-to-plate variability is a significant contributor to the overall variability of identified frequency values, more so than test-to-test variability. The lesson learned is that the numerical modeling should offer ways to account for such plate-to-plate variability.

3. FINITE ELEMENT MODELING OF THE LAMINATED COMPOSITE PLATES

A Finite Element Model (FEM) is developed to simulate the modal response of the plate and also its behavior when subjected to quasi-static loading and impact loading. The plate is meshed with 20-node quadratic hexahedra, with ten elements in each in-plane direction and one element through the thickness of each ply. Figure 8 illustrates the first four mode shapes predicted for the isotropic plate of the first code verification problem, see Section 4.

The orthotropic material properties are listed in Table 5. They have been provided by the manufacturer and some have been confirmed through coupon testing. Only the independent material properties are listed in Table 5. Constraints imposed are $E_{33}=E_{22}$, $G_{13}=G_{12}$, $\nu_{13}=\nu_{12}$, and G_{23} = 3.0 x 10^{+9} N/m^2 (kept constant).

Table 5. Statistics on material properties obtained from coupon testing.

Symbol	Mean (μ)	Standard Deviation (σ)
E_{11}	132.4 x 10^{+9} N/m^2	3% of mean
E_{22}	9.1 x 10^{+9} N/m^2	2% of mean
G_{12}	4.5 x 10^{+9} N/m^2	3.6% of mean
ν_{12}	0.30	Unknown
ν_{23}	0.40	Unknown
ρ	1,522.0 kg/m^3	2.5% of mean

Because the purpose of this work is to accurately predict the on-set and evolution of damage in the composite, elaborate constitutive and damage models are implemented. It is important to model the structure at all length scales at which damage and other forms of non-linearity may occur. These include the macro-scale, associated with the in-plane plate dimensions; the meso-scale, associated with the ply thickness; and the micro-scale, or

material length scale, associated with the fiber diameter. The non-linear, homogenization, and damage aspects of the modeling are discussed in Reference [3]. Damage modes of interest include matrix fracture, ply splitting, delamination, and fiber fracture. Special elements that use a Cohesive Zone Model as the constitutive behavior are implemented to model the ply splitting and delamination fracture surfaces. It is emphasized that none of these damage modes are exercised here; only the prediction of the linear, modal response is verified and validated.

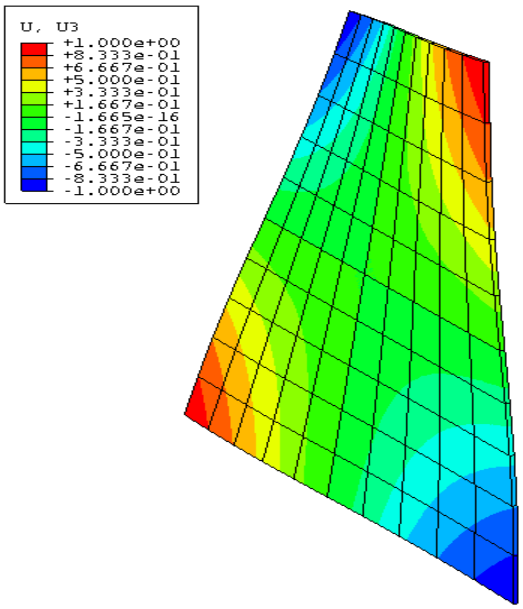

Figure 8 (a). Predicted mode shape 1.

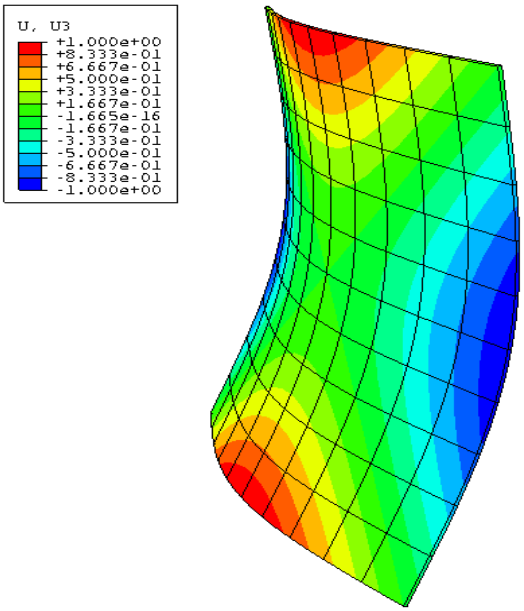

Figure 8 (b). Predicted mode shape 2.

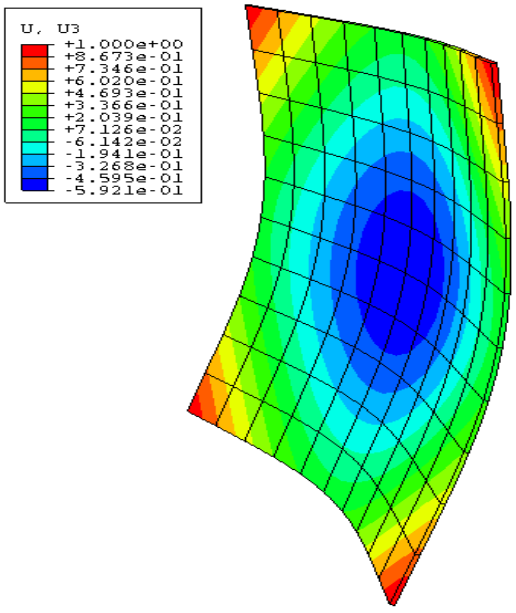

Figure 8 (c). Predicted mode shape 3.

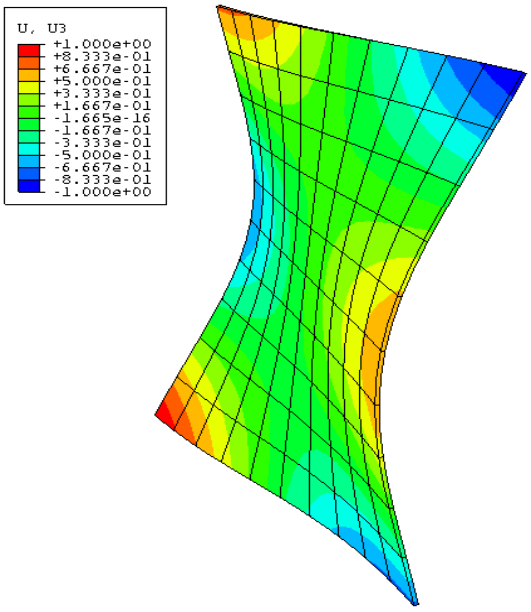

Figure 8 (d). Predicted mode shape 4.

Table 6. Modal frequencies predicted by the nominal finite element model.

Mode Number	Frequency (Hertz)	Description of the Modal Deflection Shape
1	107.49	1st torsion, no coupling
2	205.68	1st bending (2-transverse), no coupling
3	278.15	1st bending (1-fiber), 1st bending (2-transverse), coupled
4	334.05	1st bending (1-fiber), no coupling
5	411.76	1st bending (1-fiber), 1st torsion (2-transverse), coupled
6	556.74	1st bending (1-fiber), 2nd bending (2-transverse), coupled
7	583.06	2nd bending (2-transverse), no coupling
8	746.19	2nd bending (1-fiber), 2nd bending (2-transverse), coupled
9	907.81	2nd bending (1-fiber), 3rd bending (2-transverse), coupled

("1-fiber" refers to the principal direction of fibers with modulus of elasticity E_{11}, and "2-transverse" refers to the transverse direction with modulus of elasticity E_{22}.)

The first nine natural frequencies predicted by the nominal FEM are listed in Table 6. Although the model appears to be too "stiff", a good qualitative agreement can be observed between predicted frequencies in Table 6 and identified frequencies in Table 2.

4. COMPUTER CODE VERIFICATION

The computational model is implemented and analyzed using the general-purpose finite element package HKS/ABAQUS™ [4]. Computer code verification is the first step of any V&V activity. It verifies that the code is error-free for the intended purpose of the application.

The main difficulty of code verification is to obtain analytical, closed-form solutions against which calculations of the code can be verified. For this problem, the authors are only aware of two test problems as closed-form solutions can generally not be worked out with composite laminate materials and free-free boundary conditions. The first test verifies natural frequency predictions in the case of a square, free-floating, isotropic plate [5-7]. Table 7 compares the analytical and predicted natural frequencies. The plate is modeled with ten quadratic finite elements per side and one element through the thickness. Frequencies reported in Table 7 are normalized according to formulae presented in Reference [7].

Table 7. Normalized frequencies for the square, free-free, isotropic plate.

	Mode 2,2	Mode 1,3	Mode 3,1	Mode 3,2	Mode 2,3	Mode 4,1	Mode 1,4
Analytical	13.49	19.79	24.43	35.02	35.02	61.53	61.53
HKS/ABAQUS™	13.48	19.69	24.45	34.95	34.95	62.45	62.45
Error (%)	0.03	0.53	-0.05	0.20	0.20	-1.50	-1.50

(The error is calculated as analytical minus predicted, expressed in percent of the analytical value.)

The second test verifies natural frequency predictions in the case of a square, simply supported, orthotropic plate. The analytical solution is obtained from Reference [8]. Tables 8 and 9 compare the analytical and predicted natural frequencies for the cases of single-ply and three-ply laminates, respectively. In both cases, the plate is modeled with ten quadratic finite elements per side and one element through the laminate thickness. Frequencies reported in Tables 8 and 9 are normalized according to formulae presented in Reference [8].

Table 8. Normalized frequencies for the single-ply, simply supported, orthotropic plate.

	Mode 1,1 I-A	Mode 1,2 I-A	Mode 2,1 I-A	Mode 2,2 I-A	Mode 1,3 I-A	Mode 1,1 I-S	Mode 3,1 I-A
Analytical	0.047	0.103	0.119	0.169	0.189	0.217	0.218
HKS/ABAQUS™	0.048	0.104	0.121	0.173	0.192	0.217	0.225
Error (%)	-0.598	-0.971	-1.696	-1.866	-1.584	-0.002	-3.000

(The error is calculated as analytical minus predicted, expressed in percent of the analytical value.)

Table 9. Normalized frequencies for the three-ply, simply supported, orthotropic plate.

Stiffness ratio E_{x1}/E_{x2}	Density ratio ρ_1/ρ_2	Analytical	HKS/ABAQUS™	Error (%)
10	1	0.098	0.098	-0.026
15	1	0.112	0.112	-0.016
15	3	0.095	0.095	-0.015

(The error is calculated as analytical minus predicted, expressed in percent of the analytical value. The subscript 1 refers to the quantities associated with the two outer plies; the subscript 2 refers to the inner ply. Only the frequency of the first mode is shown.)

The errors reported in Tables 7, 8, and 9 verify that the potential implementation and approximation errors are several orders of magnitude smaller than the experimental variability reported in Section 2 for the first five modes. Although code verification can never provide a formal proof that the implementation is error-free, it definitely appears to be the case here. The conclusion is that, for this problem, HKS/ABAQUS™ and the implemented composite material module solve the equations correctly.

5. CONVERGENCE AND CALCULATION VERIFICATION

Calculation verification assesses the convergence of the numerical solution for the application of interest. It is also referred to as solution verification because it verifies that the discretization (mesh size and/or time step) provides a converged solution.

Solution verification relies on the assumption that the true-but-unknown solution of the continuous equations, or y_C, is equal to the approximate solution of the discretized equations, or y(h), plus an error term that is proportional to the rate of convergence:

$$y_C = y(h) + \alpha h^p + O(h^{p+1}) \qquad (4)$$

where the discretization parameter, h, represents a characteristic mesh size or time step, and the symbol p denotes the order of convergence. The main difficulty of solving equation (4) is that the continuous solution, y_C, which here represents a natural frequency, is unknown.

Solution verification is based on two techniques outlined in Reference [1]. The first one is the Grid Convergence Index (GCI) that verifies that a numerical approximation is close to the continuous solution. The order of convergence, p, is also verified. The second technique is known as the Richardson extrapolation. It estimates the continuous solution by performing an extrapolation based on several numerical approximations. Then, errors between the estimated true solution, y_C, and its numerical approximations, y(h), can be computed. Clearly, a minimum of three equations are needed to estimate the unknown triplet (y_C;p;α) in equation (4). Solution verification therefore starts by calculating the first five natural frequencies using three mesh resolutions, h_C, h_M, and h_F, such that (h_M/h_C) = (h_F/h_M) = ½. The subscripts "C", "M", and "F"

identify the coarse, medium, and fine resolutions, respectively. The order of convergence, GCI values, and Richardson extrapolation are then computed as:

$$p \approx \log\left(\frac{y(h_M)-y(h_C)}{y(h_F)-y(h_M)}\right)\Big/\log(r), \qquad GCI = 100\left|\frac{y(h_C)-y(h_M)}{y(h_C)}\right|\left(\frac{\beta}{r^p-1}\right) \tag{5}$$

$$y_C \approx \frac{r^p y(h_F) - y(h_M)}{r^p - 1} \tag{6}$$

where r denotes the ratio of successive refinements, $r = (h_C/h_M) = (h_M/h_F)$, and β is a safety factor selected such as $1 \le \beta \le 3$.[6]

The order of convergence is verified in Table 10 that also lists the GCI. Small GCI values, typically less than 1%, indicate that the approximation is close to the continuous solution. The order of convergence averaged for natural frequencies 1-5 is equal to p = 1.8, close to the value of two that should be obtained because quadratic elements are used in the analysis. The GCI values also suggest asymptotic convergence. When asymptotic converge is reached, a two-fold refinement combined with an order of convergence p should decrease the GCI by a factor of $(2)^p$. This can be observed in Table 10, for example, with the first natural frequency. From the first row, the estimated order of convergence is p = 0.82, which yields $(2)^{0.82} = 1.77$, while the ratio of GCI values is 0.91/0.52 = 1.75.

Table 10. Estimation of the order of convergence and grid convergence indices.

Mode Number	Estimated Order of Convergence	Grid Convergence Index Coarse-to-medium	Grid Convergence Index Medium-to-fine
1	0.82	0.91%	0.52%
2	2.17	0.31%	0.07%
3	1.47	0.78%	0.29%
4	2.82	0.15%	0.02%
5	1.70	0.61%	0.19%
Mean	**1.80**	**0.55%**	**0.22%**

(Results for five natural frequencies with a mesh-size refinement ratio r=2 and safety factor β=3.)

The relative errors between the Richardson extrapolation and finite element solutions are listed In Table 11. It is observed that errors are less than 1%, and that refining the mesh yields asymptotic convergence. Errors obtained from converged solutions should be reduced by a factor $(2)^p$ when the mesh size is halved. This can be observed in Table 11, for example, with the first natural frequency: $(2)^{0.82} = 1.77$, while 0.54/0.31 = 1.74 and 0.31/0.17 = 1.82. It is concluded from the solution verification study that the coarse computational mesh provides

[6] Equations (5) and (6) are given for completeness. The reader is referred to other publications listed in Reference [1] for a discussion of important caveats of using them for solution verification. In particular, the Richardson extrapolation works here because natural frequencies are integral response quantities. Equation (4) is, however, not correct in the general case because the theory of finite element stipulates that convergence is dictated by a L^p or $H^{m,n}$ norm such as $||y_C - y(h)|| = \alpha h^p + O(h^{p+1})$. Using equation (4) to estimate the convergence of a point-wise quantity, such as a local stress, may not be appropriate. Likewise, little work has been done to study the validity of equation (4) for non-linear, fast transient, or non-smooth equations; or solvers that feature automated mesh or time step refinement.

sufficiently converged estimates of the first five natural frequencies. All results presented for effect screening, meta-modeling, propagation of uncertainty, and test-analysis correlation are based on the coarse-size finite element mesh where the composite plate is discretized with ten elements per side and one element per ply through the thickness.

Table 11. Errors between numerical solutions and the Richardson extrapolation.

Mode Number	Relative Error of Coarse Solution	Relative Error of Medium Solution	Relative Error of Fine Solution
1	0.54%	0.31%	0.17%
2	0.46%	0.10%	0.02%
3	0.73%	0.26%	0.10%
4	0.35%	0.05%	0.01%
5	0.66%	0.20%	0.06%
Mean	**0.55%**	**0.18%**	**0.07%**

(The relative error is the difference between the Richardson extrapolation and finite element solution, expressed in percentage of Richardson extrapolation. Results for five natural frequencies with a mesh-size refinement ratio r=2.)

6. EFFECT SCREENING AND PARAMETER DOWN-SELECTION

The advantage of implementing a physics-based model is that it can be parameterized to describe a wide variety of configurations and materials. This comes at the cost of defining the values of a potentially large number of parameters or coefficients. It also implies that unknown input parameters introduce uncertainty that must be propagated through the simulation. Prior to propagating the uncertainty forward, we seek to better understand the relationship between input parameter variability and response feature variability. This is where design of computer experiments and effect screening methods come to play.

Input parameters introduced by the finite element and multi-scale composite models are categorized as ply orientation angles or material coefficients. It is suspected that ply angles and material properties may vary slightly from plate to plate. The effect of such variability on the natural frequencies must therefore be understood. Table 12 defines the eight ply angles and their upper and lower bounds. The variation of +/- 5 degrees around nominal orientations is an upper bound inferred from expert knowledge about how these plates are manufactured.

Table 12. Nominal values and variations of fiber orientation angles.

Symbol	Nominal	Lower Bound	Upper Bound
θ_1	0.0 degree	-5.0 degrees	5.0 degrees
θ_2	45.0 degrees	40.0 degrees	50.0 degrees
θ_3	90.0 degrees	85.0 degrees	95.0 degrees
θ_4	-45.0 degrees	-50.0 degrees	-40.0 degrees
θ_5	-45.0 degrees	-50.0 degrees	-40.0 degrees
θ_6	90.0 degrees	85.0 degrees	95.0 degrees
θ_7	45.0 degrees	40.0 degrees	50.0 degrees
θ_8	0.0 degree	-5.0 degrees	5.0 degrees

The second category of input parameters includes material coefficients needed to initialize the constitutive behavior. They are restricted to five elastic constants due to the assumption of transverse isotropy, three of which are independent. Conservative bounds of variability are

assigned in Table 13 to represent three times the standard deviation values estimated from coupon testing measurements. Also included is a varying accelerometer and cable mass that represents +/- 10% variation around the mean of the mass of transducers.

Table 13. Nominal values and variations of material properties.

Symbol	Nominal (μ)	Lower Bound	Upper Bound
E_{11}	$1.324 \times 10^{+11}$ N/m^2	(1 – 9%) x μ	(1 + 9%) x μ
E_{22}	$9.136 \times 10^{+9}$ N/m^2	(1 – 6%) x μ	(1 + 6%) x μ
G_{12}	$4.548 \times 10^{+9}$ N/m^2	(1 – 10.8%) x μ	(1 + 10.8%) x μ
ν_{12}	0.30	0.10	0.49
ν_{23}	0.40	0.10	0.49
ρ	1,522.0 kg/m^3	(1 – 7.5%) x μ	(1 + 7.5%) x μ
M_a	0.837×10^{-3} kg	(1 – 10%) x μ	(1 + 10%) x μ

Effect screening addresses the question: "*Which input parameters or combinations of inputs explain the variability of outputs?*" Screening is typically performed to determine which input parameters most influence the variability of response features. Input parameters found to have the least influence can be eliminated from the analysis by keeping them constant. Effects are screened using methods such as the analysis-of-variance [9] that performs multiple regression analyses and estimates the correlation between input effects and output features.

The data sets from which the influence of input parameters is studied are generated by analyzing the FEM for several combinations of the parameters listed in Tables 12 and 13. One can take advantage of methods for designing computer experiments to reduce the potentially large number of runs [10]. Here, extracting the first five natural frequencies of the composite plate model is not computationally expensive. Since we can afford a large number of runs, two full-factorial designs are implemented. The first design, referred to as DOE-1, evaluates all combinations of low and high ply angles while material properties are kept constant and equal to their nominal values. The second design, referred to as DOE-2, evaluates all combinations of low and high material coefficients while ply angles are kept constant and equal to their nominal values. Table 14 summarizes the properties of the two designs.

Table 14. Definition of the two designs of computer experiments.

Attribute	DOE-1	DOE-2
Purpose of the analysis	Screen ply angle effects	Screen material coefficient effects
Type of Design	Full-factorial design	Full-factorial design
Number of Variables	8 (From Table 12)	7 (From Table 13)
Number of Levels	2 (low/high)	2 (low/high)
Aliasing	No	No
Number of FEM runs	$(2)^8 = 256$ runs	$(2)^7 = 128$ runs

Only the results of main effect screening are presented in Figure 9. Main effect screening, also known as linear screening, identifies the input parameters that control the variability of output features without accounting for higher-order effects such as the coupling between two inputs. The R^2 statistic, that estimates a coefficient of correlation, is computed based on data provided by DOE-1 and DOE-2 [9]. Figure 9(a) shows the R^2 statistics obtained for the first nine natural frequencies when ply angles vary according to DOE-1. Figure 9(b) shows the R^2 statistics obtained when material coefficients vary according to DOE-2.

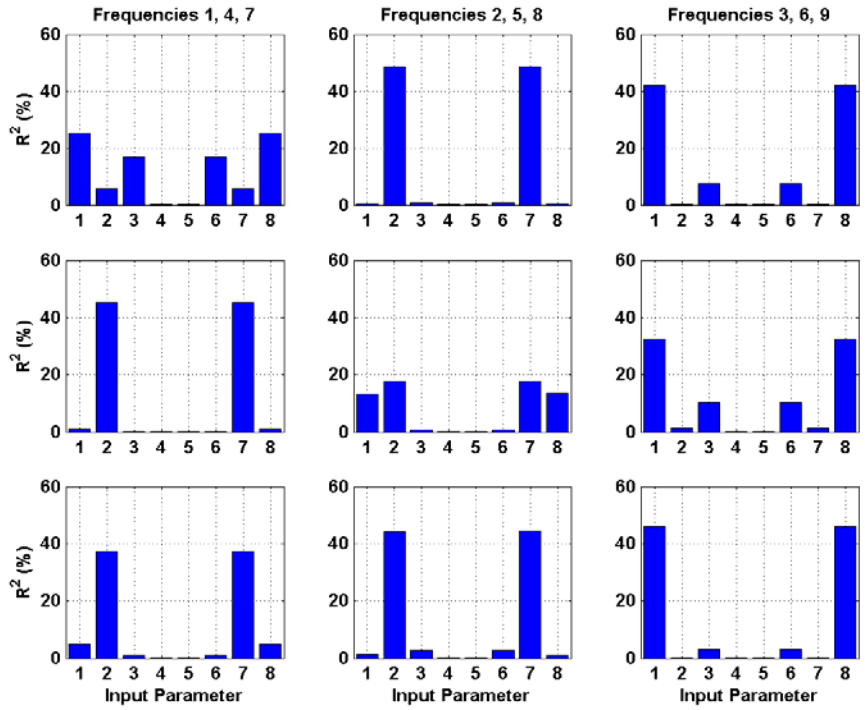

Figure 9 (a). Main effect screening from the analysis of variance of DOE-1.

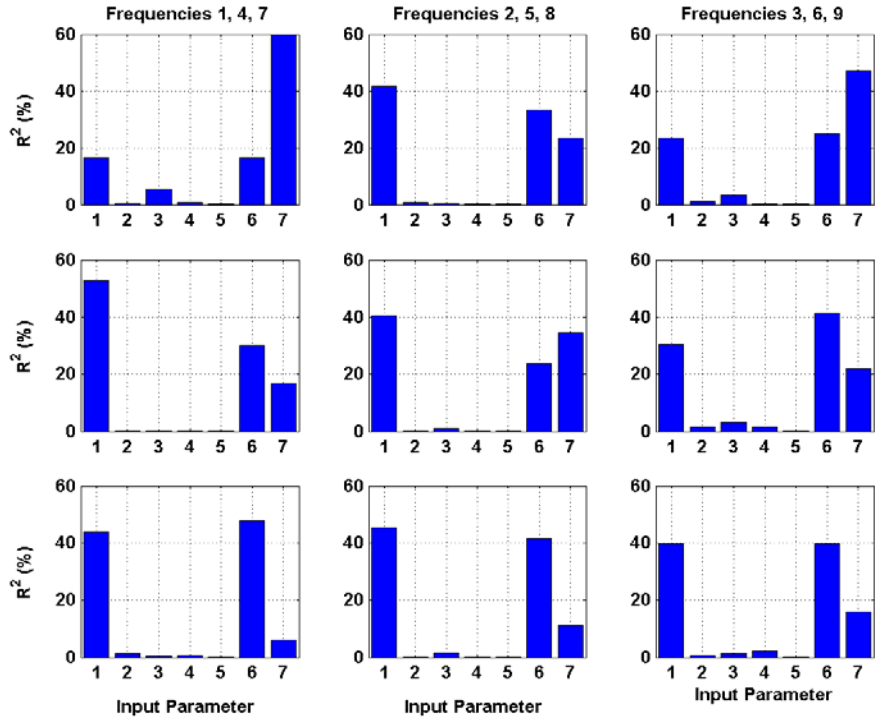

Figure 9 (b). Main effect screening from the analysis of variance of DOE-2.

In Figure 9, a large R^2 relative to the other values indicates that the corresponding input factor produces a significant variability of the natural frequency. A composite index is created for each input parameter by adding R^2 values of the first five modes. Values of the composite index are listed in Table 15. It is emphasized that this index, unlike the R^2 statistic, has no meaning other than being useful to identify overall trends across all natural frequencies.

Table 15. Composite main effect indices obtained from DOE-1 and DOE-2.

Ply Orientation Angles (DOE-1)								
θ_1	θ_2	θ_3	θ_4	θ_5	θ_6	θ_7	θ_8	Total
20.08%	24.68%	5.09%	0.08%	0.09%	5.11%	24.72%	20.15%	100.0%
Material Coefficients (DOE-2)								
E_{11}	E_{22}	G_{12}	ν_{12}	ν_{23}	ρ	M_a	Total	
37.20%	0.72%	1.88%	0.63%	0.00%	33.23%	26.34%	100.0%	

The analysis demonstrates that the variability of the five natural frequencies is controlled for the most part by four ply orientation angles (θ_1, θ_2, θ_7, θ_8), two material coefficients (E_{11}, ρ), and the added mass (M_a). Because other factors do not produce significant output variability, they are kept constant and equal to their nominal values in the remainder. To conclude, an important caveat of this analysis is briefly mentioned. The designs DOE-1 and DOE-2 have been chosen to study ply angle effect independently from material property effect because it is assumed that the geometry of the composite lay-up should be decoupled from its constitutive behavior. Further investigation (not discussed here) demonstrates that this assumption is correct for the prediction of low-frequency modes.

7. META-MODELING OF THE FINITE ELEMENT SIMULATIONS

The first objective of meta-modeling is to replace the potentially expensive FEM analysis by a fast-running surrogate that accurately captures the relationship between input parameters and a single response feature without including details of the geometry or material modeling. Polynomials are chosen as surrogates to FE models. The second objective is to verify that higher-order coupling effects are not significant, as this would invalidate the assumption made in Section 6 that ply orientation angles and material coefficients are not coupled.

Resulting from the main effect screening, only seven inputs are considered. Because fewer than the original 15 candidates are used, higher resolution designs can be considered for surrogate model fitting. A 7-factor, 3-level, full-factorial design that requires $(3)^7 = 2{,}187$ finite element runs is selected. The levels are shown in Table 16 for each input parameter.

Table 16. Input parameters retained for higher-order screening and meta-modeling.

Input Factor	Nominal	Variation	Levels
θ_1	0.0 degree	+/- 10 degrees	(-10.0; 0.0; 10.0) degrees
θ_2	45.0 degrees	+/- 10 degrees	(35.0; 45.0; 55.0) degrees
θ_7	45.0 degrees	+/- 10 degrees	(35.0; 45.0; 55.0) degrees
θ_8	0.0 degree	+/- 10 degrees	(-10.0; 0.0; 10.0) degrees
E_{11}	$1.324 \times 10^{+11}$ N/m^2	+/- 20%	$(1.0592; 1.3240; 1.5888) \times 10^{+11}$ N/m^2
ρ	1,522.0 kg/m^3	+/- 20%	(1,217.6; 1,552.0; 1,826.4) kg/m^3
M_a	0.000837 kg	+/- 20%	$(0.6696; 0.8370; 1.0044) \times 10^{-3}$ kg

Screening and model fitting are performed using the Bayesian effect screening method of Reference [11]. Because polynomials proposed to fit the data only differ by the effects that they do or do not include, such as (θ_1; E_{11}; $\theta_2 x E_{11}$; ρ^2), one can look at model fitting as a selection of effects that must be included to improve the goodness-of-fit between FEM and surrogate predictions of the natural frequencies. The Bayesian screening approach calculates the posterior probability of each effect by randomly walking from one surrogate model to the next using a Gibbs sampler. Posterior probabilities are obtained by combining, according to the Bayes rule, prior probabilities to likelihood values of fitting the data well. Prior probabilities are assigned by the analyst. Likelihood values are defined as the goodness-of-fit, for example, RMS error, between FEM natural frequencies and predictions of a polynomial surrogate.

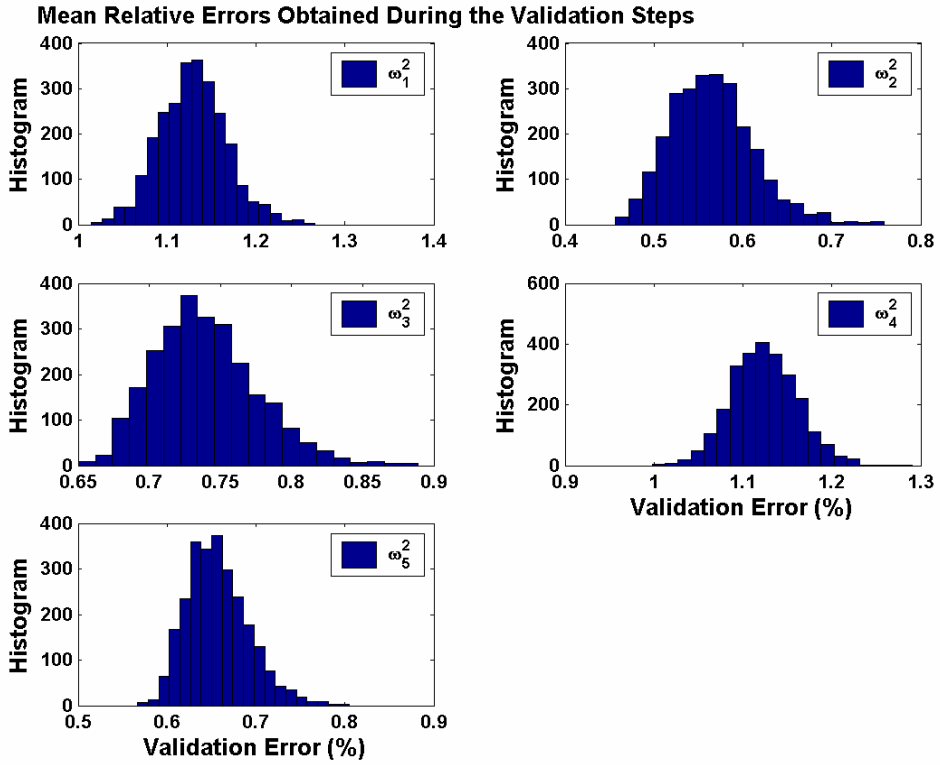

Figure 10. Accuracy of polynomials developed to predict natural frequencies 1-5.

The data sets are segregated into 1,750 runs for Bayesian screening (or training step) and 437 runs to evaluate the quality of the best polynomials (or validation step). The 437 validation runs are selected randomly. The procedure is repeated 2,600 times, each time with different training and validation data sets, to obtain fit-to-data statistics and distributions of polynomial coefficients. A small number of polynomials provide poor goodness-of-fit due to numerical ill-conditioning. The "worst" 5% of them (or 130 polynomials) are eliminated and statistics are estimated from 2,470 replicates. The distributions of prediction errors are shown in Figure 10. These are obtained from the validation step, that is, when polynomials are asked to predict frequencies that they have never seen before. The small relative errors of 1.3% at most indicate an excellent fit-to-data. The conclusion is that finite element analyses can be replaced by polynomials with little loss of prediction accuracy.

Each random walk consumes 50 iterations for the "burn-in" of the Markov chain and 200 iterations for exploring the space of all potential polynomials [11]. This means that the first 50 polynomials visited are ignored to avoid potential bias introduced by the starting point. The posterior probabilities, such as those shown in Figure 11 for predicting the first frequency, are therefore based on 2,470 x 200 = 494,000 samples. The entire procedure requests 48 hours of computing time when running MATLAB^{TM}-based algorithms on a laptop computer.

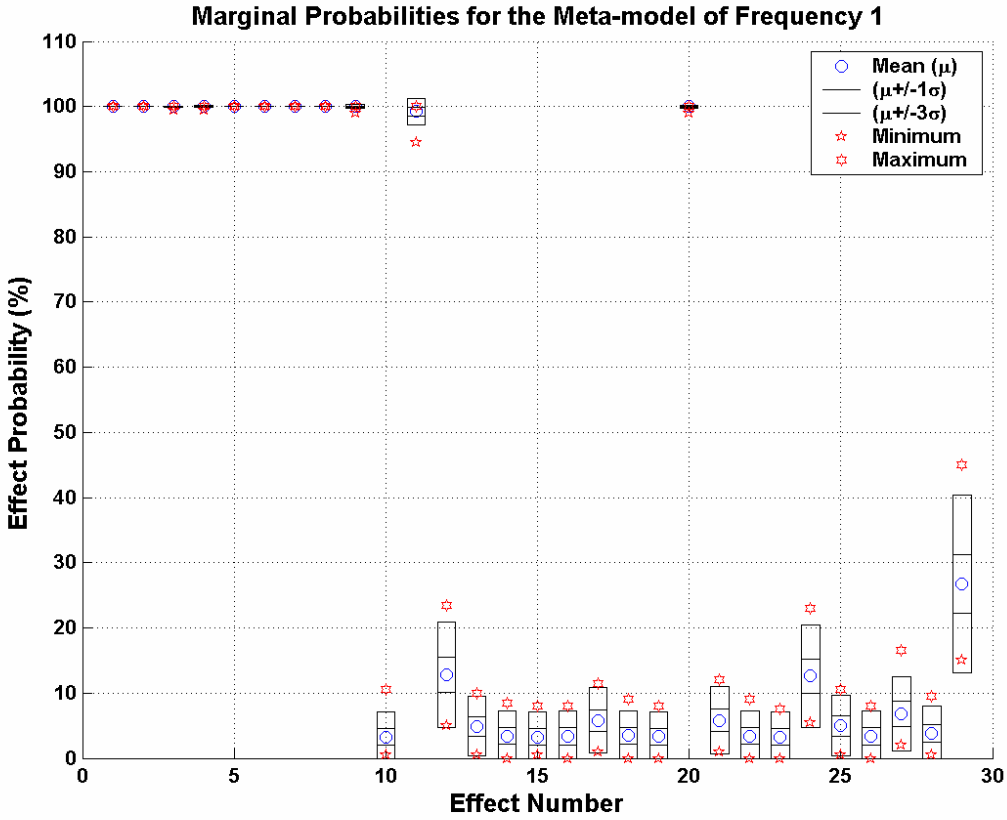

Figure 11. Posterior effect probabilities for the meta-model fitting of frequency 1.

Effects that must be included to obtain an acceptable fit-to-data are identified in Figure 11 by their large posterior probabilities.[7] Effects labeled 1 through 8 are the linear effects; effects labeled 9 through 29 are the linear interactions, such as $\theta_2 x E_{11}$ or $\rho x M_a$. Boxes represent the mean probability +/- one or three standard deviations, obtained from repeating the procedure 2,600 times with different training and validation data sets. Similar results (not presented here) are obtained for frequencies 2-5. It is verified that linear interactions and higher-order coupling between ply angles and material coefficients have little-to-no influence on the variability of the natural frequencies.

[7] Prior probabilities are set to 25% for any linear effect; 10% for an interaction given that at least one of the main effects is included; and 1% for an interaction given that none of the main effects is included. Significant effects are not necessarily those indicated by a probability close to 100%, but those that are raised above their prior probability levels.

This procedure provides a family of polynomials for each of the five natural frequencies. The results are presented for the first frequency only, and summarized by a polynomial form given in equation (7) and statistics of polynomial coefficients listed in Table 17:

$$y_1 = \beta_1 + \beta_2\theta_1 + \beta_3\theta_2 + \beta_4\theta_7 + \beta_5\theta_8 + \beta_6 E_{11} + \beta_7\rho + \beta_8 M_a + \beta_9\theta_1\theta_2 + \beta_{11}\theta_1\theta_8 + \beta_{20}\theta_2\rho + \beta_{29}\rho M_a \quad (7)$$

where y_1 is the first natural frequency and the coefficients β_k are sampled from Table 17. The input parameters are scaled between -1 and +1, therefore, the numerical values of coefficients in Table 17 indicate the importance of the corresponding effects.[8] It is further verified using Kolmogorov-Smirnov testing that the populations of coefficients are normally distributed.

Table 17. Statistics of Gaussian-distributed coefficients for meta-model of frequency 1.

Effect Number	Type of Effect	Mean (Hertz)		Standard Deviation (Hertz)	
		Value	Confidence Interval	Value	Confidence Interval
1	Mean	107.274	[107.267; 107.281]	0.103	[0.099; 0.108]
2	θ_1	-3.928	[-3.931; -3.924]	0.049	[0.046; 0.051]
3	θ_2	-1.751	[-1.754; -1.748]	0.047	[0.045; 0.049]
4	θ_7	-1.746	[-1.749; -1.743]	0.045	[0.043; 0.047]
5	θ_8	-3.929	[-3.932; -3.926]	0.048	[0.046; 0.050]
6	E_{11}	6.087	[6.084; 6.090]	0.047	[0.045; 0.050]
7	ρ	-7.342	[-7.345; -7.339]	0.049	[0.047; 0.051]
8	M_a	-3.570	[-3.573; -3.567]	0.045	[0.043; 0.047]
9	$\theta_1 \times \theta_2$	1.682	[1.679; 1.686]	0.055	[0.052; 0.058]
11	$\theta_1 \times \theta_8$	-1.378	[-1.382; -1.375]	0.057	[0.055; 0.060]
20	$\theta_2 \times \rho$	1.682	[1.678; 1.686]	0.058	[0.055; 0.061]
29	$\rho \times M_a$	0.725	[0.721; 0.729]	0.061	[0.058; 0.064]

(The 99% confidence intervals are shown. Distributions assumed to be Gaussian.)

It is concluded that polynomial meta-models can be trained to replace the finite element simulations and predict the first five natural frequencies. The preliminary down-selection of main effects is verified. The prediction accuracy of meta-models is quantified. Distributions of polynomial coefficients are obtained that account for the model fitting uncertainty.

8. PROPAGATION OF UNCERTAINTY FROM INPUTS TO OUTPUTS

Because we are lacking knowledge about some aspects of the modeling and simulation, the uncertainty must be propagated in order to make predictions. The uncertainty considered here includes variability of the ply orientation angles and lack-of-knowledge about the material properties. Because we have taken the path of substituting statistical meta-models for the FE simulations, the model fitting uncertainty must also be accounted for.

[8] The meta-model defined by equation (7) lists a term ($\theta_2\rho$) that represents the interaction between the second ply angle and density. This interaction is perfectly legitimate here because a full-factorial design of computer experiments is used to develop the surrogate meta-model. However, it seems to contradict the statement made in Section 6 that ply angles do not interact with material properties. Since this interaction is the only one found and it has little overall influence over predictions of the meta-model, as indicated by the small coefficient value of 1.682 Hertz in Table 17, it is not deemed necessary to revisit the assumption of non-interaction between ply angles and material properties.

Since the ply angles and material properties are suspected to vary from plate to plate, the variability of natural frequency can be obtained by assuming probability distributions for the input parameters and propagating them to the output responses. For simplicity and because evaluating meta-models is inexpensive, Monte Carlo sampling is implemented for uncertainty propagation. Monte Carlo simulations are performed with 10^{+4}, 10^{+5}, 10^{+6}, and 10^{+7} samples to verify convergence of the output statistics. A thorough study of the order of convergence of confidence intervals concludes that 10^{+5} runs provide acceptable statistics. The effects of input distribution and correlation structure on output statistics are also investigated. Although the results are not presented here, these factors have a significant influence [2]. This indicates that analysts should not make assumptions that may not be warranted by what is truly known.

The results presented combine input parameter variability to model fitting uncertainty. A thousand meta-models are generated by sampling the polynomial coefficients using normal distributions whose hyper-parameters are listed in Table 17. With each meta-model, 1,000 combinations of input parameters are evaluated using the uncorrelated uniform distributions defined in Table 18. This results in a total of 10^{+6} Monte Carlo runs. The principle of indifference is invoked here to define uniform distributions because no information is available to indicate how the ply angles and material properties may vary.

Table 18. Definition of uncorrelated, uniform input parameter distributions.

Input Variable	Minimum	Maximum	Range of Variation
θ_1	-9.0 degrees	9.0 degrees	+/- 9.0 degrees of nominal
θ_2	36.0 degrees	54.0 degrees	+/- 9.0 degrees of nominal
θ_7	36.0 degrees	54.0 degrees	+/- 9.0 degrees of nominal
θ_8	-9.0 degrees	9.0 degrees	+/- 9.0 degrees of nominal
E_{11}	$1.059 \times 10^{+11}$ N/m^2	$1.589 \times 10^{+11}$ N/m^2	+/- 10% of nominal
ρ	1,218.0 kg/m^3	1,826.0 kg/m^3	+/- 10% of nominal
M_a	0.000669 kg	0.001000 kg	+/- 10% of nominal

Table 19 lists the first four statistical moments (mean, standard deviation, skewness, and kurtosis) of the populations of natural frequencies. A histogram is shown in Figure 12 for the first natural frequency that approximates its unknown distribution. The fit-to-data of a normal distribution (continuous curve) is compared to the empirical histogram in Figure 12.

Table 19. Statistics of frequencies 1-5 obtained from 10^{+6} Monte Carlo runs.

Mode Number	Mean (Hertz)	Standard Deviation (Hertz)	Skewness (Unit-less)	Kurtosis (Unit-less)
1	107.473	6.665	0.103	2.744
2	206.642	15.846	0.043	2.555
3	281.155	19.798	0.120	2.733
4	329.032	24.838	0.136	2.404
5	407.985	27.901	0.140	2.395

Observation of Table 19 and Figure 12 indicates that the output distribution of frequency 1 is not Gaussian. For example, the skewness and kurtosis indicate non-Gaussian behavior since they should be equal to zero and three, respectively, for a perfectly normal distribution. This trend is verified in Figure 13 that shows the normal probability plots for the distributions of five frequencies. Gaussian curves should be aligned on a straight line, which is not the case at

the tails of the distributions. The results indicate that the output variability cannot be described using Gaussian laws, and an alternate representation of uncertainty is briefly discussed next.

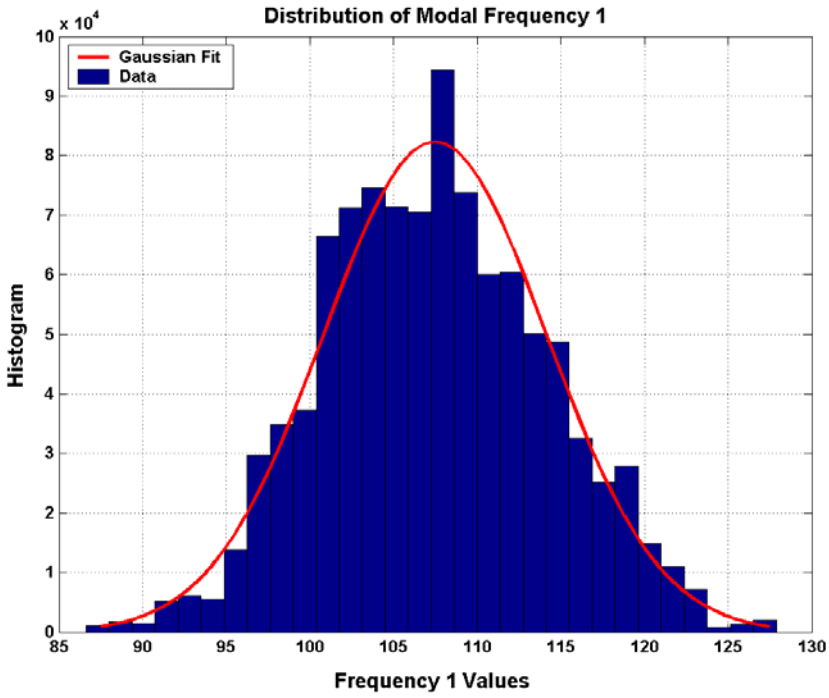

Figure 12. Histogram of frequency 1 values obtained from 10^{+6} Monte Carlo runs.

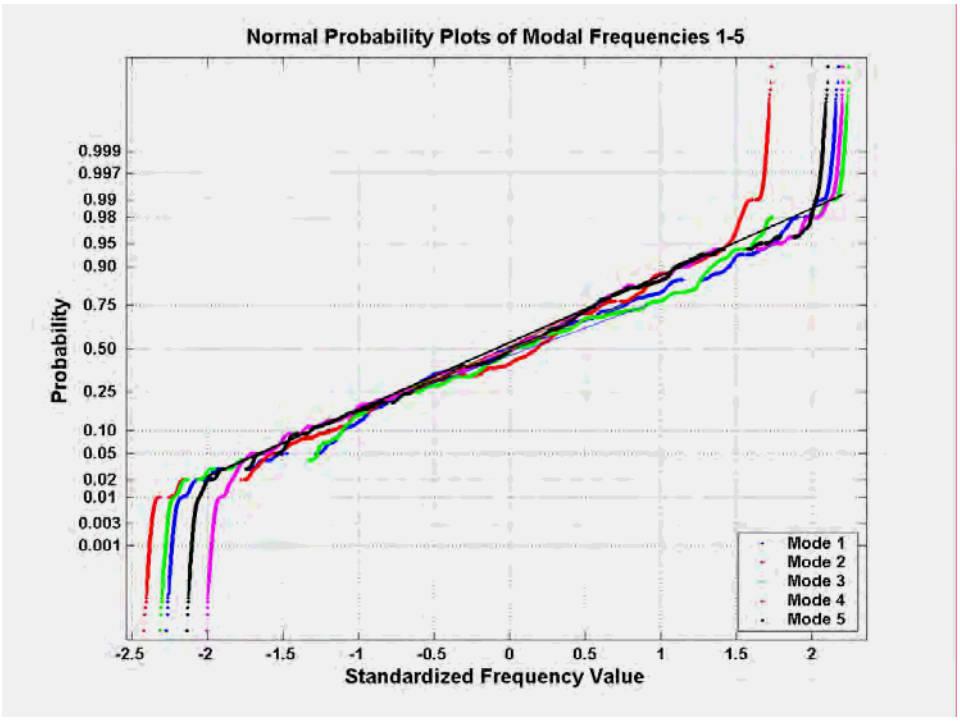

Figure 13. Normal probability plots for the distributions of frequencies 1-5.

Two distinct types of uncertainty have been combined so far. The first one is the variability of ply angles and material properties. The second one is the meta-model fitting uncertainty. While it has been shown that the second type of uncertainty is normally distributed, this is not known of the first type. Therefore, it may be incorrect to assume probability distributions for the ply angles and material properties when no evidence suggests how these truly vary.

Because the populations of polynomial coefficients have been thoroughly characterized, it is legitimate to sample their normal distributions. On the other hand, modeling the lack-of-knowledge about the geometry and material using any probability distribution is assuming more than truly known. It is proposed to characterize this lack-of-knowledge with minimum and maximum bounds, and propagate intervals from ply angles and material properties to the five natural frequencies.

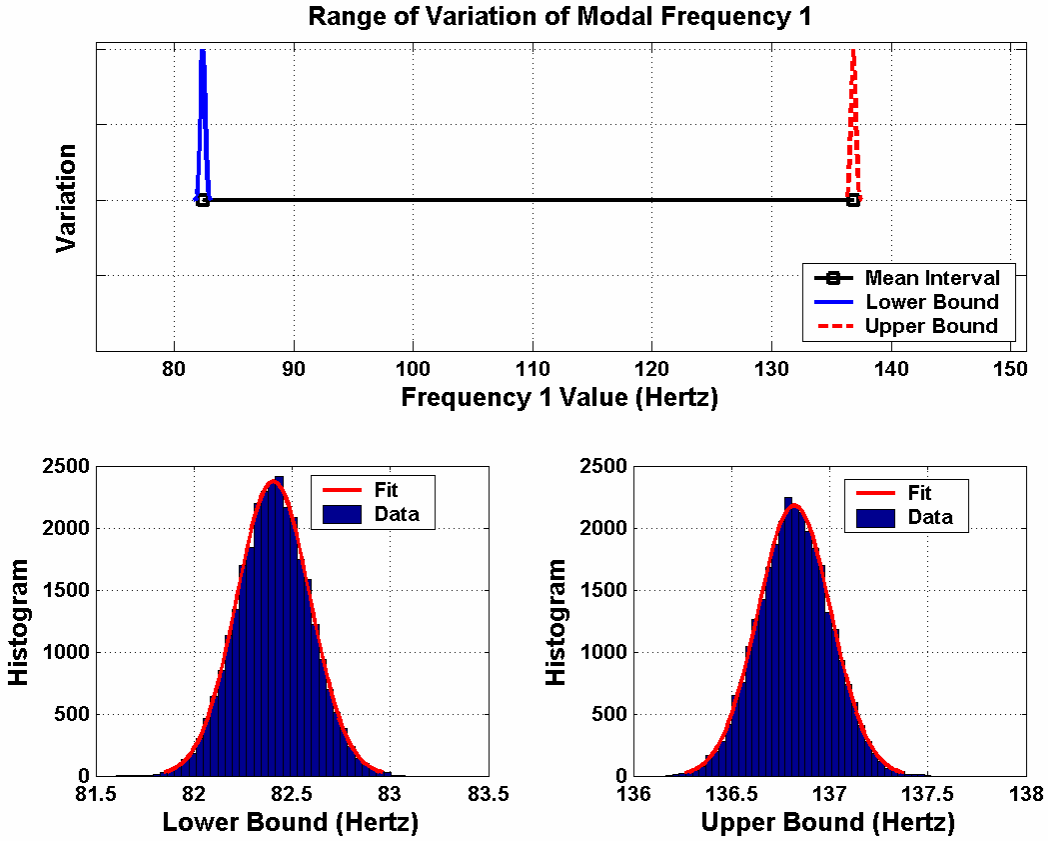

Figure 14. Interval with randomly distributed end-points for natural frequency 1.

The calculation starts, as before, by randomly generating 3 x 10^{+4} meta-models using the normal distributions defined in Table 17. For each meta-model, two optimization problems are solved to propagate the intervals of input parameters. Numerical optimization searches for the minimum and maximum natural frequencies given that each input parameter is bounded. The input parameter bounds are set to +/- 10% of their nominal values, as shown in Table 18. It is emphasized that the bounds no longer define a probability distribution but, instead, impose constraints for the numerical optimization. This procedure hence combines the Monte Carlo sampling of polynomial meta-models to the propagation of input parameter intervals. Because

the polynomials are well-behaved and inexpensive functions, each optimization convergences in less than seven iterations and the computational cost is insignificant. The procedure yields a population of intervals for each natural frequency. The results are presented in the form of an interval with randomly distributed end-points, such as illustrated in Figure 14 for the first mode.

It is verified that the populations of lower and upper interval end-points for the five natural frequencies follow Gaussian probability laws whose statistics are provided in Table 20. The skewness and kurtosis values are very close to zero and three, respectively, and excellent goodness-of-fit is obtained with normal probability laws, as illustrated in Figure 14. Also, the lower and upper end-points of frequency intervals can be compared to the mean and standard deviation values obtained in Table 19 via pure Monte Carlo sampling. The "true" minimum and maximum values of end-points in Table 20 are between three and four standard deviations away from the mean statistics listed in Table 19. This implies that a very large number of Monte Carlo samples would be needed to estimate the lower and upper end-points with good accuracy. Combining meta-model sampling to interval propagation is therefore computationally more efficient than a pure sampling approach.

Table 20. Statistics of the upper and lower end-points of frequency intervals.

Lower End-points of Frequency Intervals						
Mode Number	**Minimum (Hertz)**	**Maximum (Hertz)**	**Mean (Hertz)**	**Std. Deviation (Hertz)**	**Skewness (Unit-less)**	**Kurtosis (Unit-less)**
1	81.606	83.076	82.404	0.185	-0.012	3.019
2	151.440	153.831	152.773	0.274	-0.013	3.052
3	208.641	212.064	210.495	0.385	0.023	3.023
4	254.716	258.838	256.803	0.519	0.003	3.018
5	327.414	331.359	329.363	0.493	-0.015	3.002
Upper End-points of Frequency Intervals						
Mode Number	**Minimum (Hertz)**	**Maximum (Hertz)**	**Mean (Hertz)**	**Std. Deviation (Hertz)**	**Skewness (Unit-less)**	**Kurtosis (Unit-less)**
1	136.165	137.516	136.820	0.185	0.021	2.979
2	263.265	265.500	264.357	0.274	-0.005	2.988
3	356.923	360.280	358.738	0.384	-0.012	2.979
4	402.380	406.563	404.554	0.518	-0.008	2.973
5	488.051	491.990	489.813	0.493	0.004	2.980

(The minimum, maximum, mean, standard deviation, skewness, and kurtosis statistics are estimated from a population of 30,000 frequency intervals. Each frequency interval is obtained for a given meta-model. Lower and upper frequency bounds are calculated by optimization when input parameters are contained within the intervals defined in Table 18.)

The uncertainty quantification study demonstrates that issues such as the type of input distribution, its correlation structure, and the number of samples drawn from the distributions can have a significant influence on the statistics of response features [2]. In particular, analysts are warned against the temptation of assuming more than is truly known. For this application, prediction uncertainty is best characterized as an interval of natural frequency values with randomly distributed end-points, which is not without similarity with the recently developed concept of lack-of-knowledge proposed to model uncertainty in linear, modal dynamics [12].

9. TEST-ANALYSIS CORRELATION

Test-analysis correlation is usually where conclusions about the prediction accuracy of the model are drawn from comparing measurements to predictions. In this study, the agreement between identified and predicted natural frequencies is assessed using quantitative metrics. It is also shown that parameters of the model can be calibrated to improve the correlation. An alternative to calibration for assessing the accuracy of predictions is illustrated by aggregating the sources of testing and modeling uncertainty instead of using measurements to calibrate parameters of the model.

Statistics of the measured and predicted natural frequencies are summarized in Table 21. Measurements come from the testing presented in Section 2, see Table 2. Predictions result from the propagation of uncertainty discussed in Section 8, see Table 19. The frequencies are predicted by combining a thousand meta-models and a thousand samples of uncorrelated, uniformly distributed combinations of ply angles and material coefficients. It is observed from Table 21 that predictions are systematically stiffer than measurements. The comparison also shows that the predicted standard deviations are five to eight times larger than the measured standard deviations. This tends to indicate that the assumption made of +/- 10% variability of input parameters relative to their nominal values is too conservative.

Table 21. Statistics of measured and predicted modal frequencies 1-5.

Mode Number	Identified Frequency		Predicted Frequency	
	Mean	Standard Deviation	Mean	Standard Deviation
1	107.37 Hertz	1.05 Hertz (0.98%)	107.47 Hertz	6.67 Hertz (6.20%)
2	191.81 Hertz	2.37 Hertz (1.24%)	206.64 Hertz	15.85 Hertz (7.67%)
3	274.06 Hertz	2.92 Hertz (1.07%)	281.16 Hertz	19.80 Hertz (7.04%)
4	315.31 Hertz	3.13 Hertz (0.99%)	329.03 Hertz	24.84 Hertz (7.55%)
5	398.88 Hertz	3.00 Hertz (0.75%)	407.99 Hertz	27.90 Hertz (6.84%)

(Numbers between parentheses are standard deviations given as percentages of mean values.)

The next step is to calculate test-analysis correlation metrics. Metrics are important to offer a quantitative assessment of prediction accuracy, as well as define the objective functions needed for model calibration. The simplest test-analysis correlation metrics are those whose definition restricts them to the analysis of a single response feature. Examples include the absolute error, relative error, and T-test:

$$e = y^{Test} - y\,, \qquad e = \frac{y^{Test} - y}{y^{Test}}\,, \qquad e = \frac{y^{Test} - y}{\sigma_y^{Test}} \tag{8}$$

where y^{Test} and y denote single measured and predicted features. The T-test for significantly different means accepts or rejects the hypothesis that the predicted feature y comes from the same parent distribution as the population of measured features represented by the mean y^{Test} and standard deviation σ_y^{Test}.

A second category of metrics offers more generality by handling multiple features at once. Examples are the Root Mean Square (RMS) error and the Mean Square Error (MSE):

$$e = \sqrt{\frac{1}{N_F}\sum_{k=1\ldots N_F}\left(y_k^{Test} - y_k\right)^2}\,, \qquad e = \frac{1}{N_F}\sum_{k=1\ldots N_F}\left(\frac{y_k^{Test} - y_k}{\sigma_k^{Test}}\right)^2 \tag{9}$$

where N_F denotes the number of response features, for example N_F = 5 natural frequencies here. The RMS error makes sense only if physical quantities with similar units are combined. The MSE does not suffer from this disadvantage because of the normalization by standard deviations. A good match is indicated by small MSE values, typically less than 1%.

Multivariate statistics are the most general metrics for test-analysis correlation because they can handle populations of physically dissimilar response features. Two examples are the Mahalanobis distance and Kullback-Leibler entropy:

$$e = \left(y^{Test} - y\right)^T \left(S_{yy}^{Test}\right)^{-1} \left(y^{Test} - y\right) \tag{10-a}$$

$$e = \left(y^{Test} - y\right)^T \left(S_{yy}^{Test}\right)^{-1} \left(y^{Test} - y\right) + \frac{1}{2}\left\{ \text{Trace}\left[\left(S_{yy}\right)\left(S_{yy}^{Test}\right)^{-1}\right] - \log\left(\frac{\det\left(S_{yy}\right)}{\det\left(S_{yy}^{Test}\right)}\right) - N_F \right\} \tag{10-b}$$

where N_F is the number of response features; y^{Test} and y now denote vectors of measured and predicted features; and S_{yy}^{Test} and S_{yy} represent matrices of measured and predicted variance and covariance coefficients. The Mahalanobis distance generalizes the T-test to multivariate statistics. It is combined with the Hotelling T^2-test to assess the confidence level with which the vector of predictions estimates the mean vector of measurements. The multivariate Kullback-Leibler entropy in equation (10-b) assumes Gaussian distribution laws.

The test-analysis correlation metrics of equations (8-10) are listed in Table 22. Metrics are calculated from the mean and standard deviation statistics listed in Table 21. With an error that averages 3.41% only, the prediction accuracy is deemed acceptable for the intended purpose.

Table 22. Test-analysis correlation metrics for modal frequencies 1-5.

Univariate Test-analysis Correlation Metrics			
Mode Number	**Absolute Error**	**Relative Error**	**T-test Statistic**
1	-0.10 Hertz	-0.09%	-0.10
2	-14.83 Hertz	-7.73%	-6.26
3	-7.09 Hertz	-2.59%	-2.43
4	-13.72 Hertz	-4.35%	-4.38
5	-9.10 Hertz	-2.28%	-3.03

Multivariate Test-analysis Correlation Metrics		
Type of Metric	**Unit**	**Value**
Root Mean Square (RMS) error, defined in equation (9)	Hertz	4.26 Hertz
Mean Square Error (MSE), defined in equation (9)	Unit-less	14.70
Multivariate Mahalanobis distance, defined in equation (10-a)	Unit-less	73.06
Multivariate Kullback-Leibler entropy, defined in equation (10-b)	Unit-less	144.04

The next step is to calibrate the ply angles and material coefficients to improve the test-analysis correlation. This can be achieved in a number of ways that are overviewed, for example, in Reference [13]. We chose to formulate an optimization problem where the MSE is minimized given constraints defined in Table 18. The agreement between measurements and predictions of the pre-calibrated and post-calibrated models is illustrated in Table 23. Pre-calibrated predictions are those obtained when the "mean" meta-model is evaluated using the nominal input parameters of Table 16. Post-calibrated predictions are made with the calibrated

parameter values of Table 24. The "mean" model refers to the polynomial defined by the mean coefficients such as those shown in Table 17 for the first mode. It is emphasized that the meta-models to predict natural frequencies 1-5 are kept constant during numerical optimization; only the ply angles and material properties are optimized.

Table 23. Test-analysis correlation obtained with the nominal and calibrated models.

Mode Number	Identified Frequency	Nominal Meta-model		Calibrated Meta-model	
		Frequency	Error	Frequency	Error
1	107.4 Hertz	107.5 Hertz	-0.09%	107.4 Hertz	-0.00%
2	191.8 Hertz	206.6 Hertz	-7.73%	192.1 Hertz	-0.18%
3	274.1 Hertz	281.2 Hertz	-2.59%	274.1 Hertz	+0.00%
4	315.3 Hertz	329.0 Hertz	-4.35%	317.5 Hertz	-0.70%
5	398.9 Hertz	408.0 Hertz	-2.28%	396.8 Hertz	+0.52%

(The relative errors are calculated according to equation (8) and given in percentage of the test values.)

Table 24. Nominal and calibrated values of the ply angles and material properties.

Input Parameter	Nominal Value	Constraint		Calibration	
		Lower	Upper	Value	Scaling
θ_1	0.0	-9.0	9.0	-5.2	-0.58
θ_2	45.0	36.0	54.0	38.7	-0.70
θ_7	45.0	36.0	54.0	46.8	+0.20
θ_8	0.0	-9.0	9.0	4.3	+0.48
E_{11}	$1.324 \times 10^{+11}$	$1.059 \times 10^{+11}$	$1.589 \times 10^{+11}$	$1.414 \times 10^{+11}$	+0.34
ρ	1,522.0	1,218.0	1,826.0	1,826.0	+1.00
M_a	0.000837	0.000669	0.001000	0.000669	-1.00

(Units are: degree for θ_1, θ_2, θ_7, θ_8; N/m^2 for E_{11}; kg/m^3 for ρ; and kg for M_a. The "Scaling" column is the calibration value scaled in [-1; +1] where -1 and +1 are the lower and upper constraints, respectively.)

The pre-calibration MSE of 14.70 reported in Table 22 is reduced to 0.20 and Table 23 shows that the measured frequencies can be reproduced with high accuracy. Input parameters listed in Table 24 receive adjustments that stay within the constraints imposed of +/- 10% variation relative to the nominal values, except for ρ and M_a. The density and accelerometer mass parameters reach the upper and lower bounds, respectively. The physical validity of adjustments brought to ρ and M_a is questioned since it has been established from Table 21 that the 10% bounds are already too large (that is, they produce too much natural frequency variability compared to the one measured).

What this exercise illustrates is simply that the measured features can be matched by a calibrated model. It is our opinion that calibration offers little interest, as far as validating a model is concerned, because obtaining calibrated solutions is conditioned on choices that include the nature of response features, test-analysis metric, optimization solver, starting point, constraints, and feasibility to identify the global minimum.

An alternative to model calibration is presented next based on the recently developed concept of total uncertainty [14, 15]. When a model is calibrated, the test data sets and their uncertainty are employed in an inverse inference problem to optimize the model parameters. A different approach is to aggregate all sources of information and assess the total uncertainty represented by the testing and modeling evidence. A Total Uncertainty (TU) metric has been proposed to quantify the degree to which several sources of information are consistent with

one another, relative to the two extreme cases of absolute certainty and complete uncertainty. While a few equations are summarized here for completeness, details about the motivation and derivations can be obtained from References [14] and [15].

TU metric calculations start by collecting mathematical descriptions of uncertainty in a so-called information matrix, $H_{m,N}$, and performing its Singular Value Decomposition (SVD):

$$H_{m,N} = \begin{bmatrix} h_{1,1} & h_{1,2} & \cdots & h_{1,N} \\ \vdots & \vdots & \cdots & \vdots \\ h_{i,1} & h_{i,2} & \cdots & h_{i,N} \\ \vdots & \vdots & \cdots & \vdots \\ h_{m,1} & h_{m,2} & \cdots & h_{m,N} \end{bmatrix}, \qquad H_{m,N} = U \Sigma V^T, \qquad \Sigma = \begin{bmatrix} \sigma_1 & & 0 \\ & \ddots & \\ 0 & & \sigma_N \end{bmatrix} \tag{11}$$

where m denotes the number of discretization bins (number of rows) and N is the number of distributions (number of columns). The column $\{h_{i,j}\}$ represents the j^{th} uncertainty distribution of a response feature y. Choices of mathematical representation of uncertainty include probability density functions, possibility distributions, intervals, Dempster-Schafer belief functions, random sets, fuzzy membership functions, imprecise probabilities [14, 15]. Multiple representations of uncertainty can be combined in $H_{m,N}$, as well as multiple features, and representations originating from multiple sources of evidence such as testing, modeling, and expert judgment.

By analogy with the use of SVD in signal processing or Structural Dynamics, the singular values $\sigma_1, \sigma_2, \ldots, \sigma_N$ characterize the amount of uncertainty and the consistency of information included in matrix $H_{m,N}$. The TU metric is defined as:

$$TU = N\left(\frac{\sum_{j=1}^{N} \sigma_j^2}{\sum_{j=1}^{N} h_{max,\,j}^2} - 1 \right) \tag{12}$$

where $h_{max,j}$ denotes the maximum value of the j^{th} column. The definition (12) produces values scaled between zero and an upper bound $TU_{Max} = N(m-1)$ that only depends on the size of the information matrix. The ratio (TU/TU_{Max}) is a positive number scaled between zero and one. It can be verified that zero means absolute certainty and one means complete uncertainty [14].

Results of applying the concept of total uncertainty to the test and simulation data sets are presented in Table 25. Five information matrices $H_{50,2}$ are generated, one for each natural frequency. The first column stores a histogram of measured values. The second column stores a histogram of predicted values. Histograms approximate the unknown probability distributions and they are discretized into m = 50 bins, which yields $TU_{Max} = 98$. TU values in Table 25 are computed according to equations (11-12). The last column shows what the TU values would be if the distributions of measured and predicted frequencies were described by continuous Gaussian laws whose hyper-parameters are listed in Table 21. The average value is only 19.7%, or 16.0% if Gaussian probability density functions are assumed, which indicates small total uncertainty and reasonable consistency between the measured and predicted data sets.

Table 25. TU metrics for the measured and predicted natural frequencies 1-5.

Mode Number	TU Metric Values (Unit-less)	(TU/TU_{Max}) From Empirical Distributions	(TU/TU_{Max}) From Gaussian Distributions
1	18.4	18.7%	15.7%
2	21.2	21.6%	15.9%
3	18.7	19.1%	16.2%
4	18.9	19.3%	15.9%
5	19.5	19.9%	16.1%

(TU values are computed with matrices of empirical histograms for the measured and predicted natural frequencies. Based on m = 50 bins, N = 2 histograms, and TU_{Max} = 98.)

One final result is briefly discussed, when the testing and modeling sources of information about the five natural frequencies are aggregated into a single matrix, $H_{100,10}$. Columns store the two histograms of measured and predicted natural frequencies for each of the five modes. Based on N = 10 columns and a discretization into m = 100 bins, one obtains TU = 171.3, TU_{Max} = 990, and (TU/TU_{Max}) = 17.3%, which is consistent with results in Table 25 and offers the advantage of a single, compact metric. Aggregating information obtained from testing and modeling for several response features illustrates the multivariate potential of the TU metric.

It is emphasized that the TU metric is not a goodness-of-fit indicator. It is used to assess the degree of consistency of information obtained from different sources, such as testing and modeling here, but it does not replace test-analysis correlation metrics. The importance of a quantification of total uncertainty stems from the fact that, to decide whether or not it would be beneficial to spend additional resources refining the model or calibrating its parameters, one should examine the agreement between measurements and predictions relative to uncertainty, and not in a vacuum like it is usually done.

10. FINAL ASSESSMENT OF PREDICTION ACCURACY

This publication discusses the results of a V&V study for the modeling of multi-layered composite plates. The response features of interest are the first five natural frequencies. Test repeatability, mesh convergence errors, parametric variability, model fitting uncertainty, and test-analysis correlation are thoroughly quantified. In this Section, a final statement is made about the predictive accuracy of the composite model and the level of confidence with which modal frequency predictions can be made for a potentially different multi-layered configuration.

Table 26 summarizes the quantification of the sources of uncertainty. For simplicity, the statistics are averaged over the five natural frequencies. An error model can be proposed to aggregate the sources of modeling error and variability. Here, a simple average of statistics for solution convergence $(\mu_1;\sigma_1)$, model fitting $(\mu_2;\sigma_2)$, and parametric variability $(\mu_3;\sigma_3)$ is proposed:

$$\mu_T = \mu_1 + \mu_2 + \mu_3, \qquad \sigma_T^2 = \sigma_1^2 + \sigma_2^2 + \sigma_3^2 \tag{13}$$

The total error model (13) yields statistics μ_T = 3.64 Hertz and σ_T = 19.02 Hertz. These are compared to the statistics of test-analysis correlation in Table 26, where μ_C = 8.97 Hertz and σ_C = 19.18 Hertz. Two observations are made. First, a discrepancy of $(\mu_C - \mu_T)$ = 5.33 Hertz is found between the error model (13) and the error inferred from test-analysis correlation. The difference is due to the modeling error, that is, the error made when the composite model is

substituted to reality. It is a source of error that one should not attempt to reduce by calibrating parameters of the model because it is inherent to the modeling assumptions.

Second, the predicted variability of frequencies, σ_T = 19.02 Hertz, is several times larger than the value of σ_4 = 2.49 Hertz measured experimentally. The simulation variance comes for the most part from the variability of ply angles and material properties, which could be reduced through parameter calibration or better characterization of the geometry and material.

Table 26. Summary of the quantification of testing and modeling uncertainty.

Source of Uncertainty	Statistics		Evidence
	Mean (μ)	Std. Deviation (σ)	
Code Error, Solution Convergence	μ_1 = 1.49 Hertz	σ_1 = 0.87 Hertz	Table 11
Meta-model Fitting Error	μ_2 = 2.15 Hertz	σ_2 = 0.18 Hertz	Figure 10
Model Parameter Variability	μ_3 = 0.00 Hertz	σ_3 = 19.00 Hertz	Table 19
Experimental Variability	μ_4 = 0.00 Hertz	σ_4 = 2.49 Hertz	Table 2
Test-analysis Correlation	μ_C = 8.97 Hertz	σ_C = 19.18 Hertz	Table 21

(The systematic bias from code verification is accounted for in the solution convergence uncertainty. Likewise, experimental variability is rolled into the statistics of test-analysis correlation.)

From these observations, it is concluded that the prediction error (μ +/- σ) can be reduced to μ = 5.33 Hertz +/- σ = 2.49 Hertz at the 68% (or one standard deviation, σ) confidence level. This would require a better characterization of the composite lay-up and material properties to reduce the variability of input parameters. Parameter calibration can also be employed to infer the input parameter variability from experimental observations. Because the prediction error is small relative to the magnitude of natural frequencies, the composite model is validated with sufficient accuracy to simulate the linear, elastic, low-frequency response of the plates.

We are also confident that natural frequencies for different multi-layered configurations can be predicted with a similar degree of accuracy as long as the same modeling rules are followed. These rules include: modeling each individual ply with one element through the thickness; maintaining an acceptable aspect ratio of elements; adjusting the time step to the element size to guarantee accuracy with an explicit time integration scheme; verifying that the mesh and time step provide a converged solution; and thoroughly characterizing the ply angle and material property variability.

ACKNOWLEDGEMENTS

The authors acknowledge the continuing support and encouragement of Scott Doebling, X-DO and leader of the ASC V&V program; and Mark Anderson, ESA-WR and leader of the ASC Engineering V&V program element. ASC is the Advanced Scientific Computing program of the U.S. Department of Energy. Funding for this work was also provided by the Laboratory Directed Research and Development (LDRD) project for Damage Prognosis, lead by Charles Farrar, ESA-WR. The technical advice and guidance of Jane Booker, ESA-WR, and Todd Williams, T-3, at Los Alamos National Laboratory is acknowledged and greatly appreciated.

REFERENCES

[1] Hemez, F.M., Doebling, S.W., Anderson, M.C., "A Brief Tutorial on Verification and Validation," *22nd SEM International Modal Analysis Conference*, Dearborn, Michigan,

January 26-29, 2004. Available as unlimited, public release LA-UR-03-8491 of the Los Alamos National Laboratory, Los Alamos, New Mexico.

[2] Hemez, F.M., Tippetts, T., Salazar, I., "Composite Model Verification and Validation for Damage Prognosis," *Internal Report*, Los Alamos National Laboratory, Los Alamos, New Mexico, October 2004 (in preparation).

[3] Tippetts, T., Hemez, F.M., "Non-linear Models of Composite Laminates," *23rd SEM International Modal Analysis Conference*, Orlando, Florida, January 31-February 3, 2005. Available as unlimited, public release LA-UR-04-8100 of the Los Alamos National Laboratory, Los Alamos, New Mexico.

[4] Abaqus™/Explicit, User's Manual, Version 6.2, Hibbitt, Karlsson & Sorensen, Pawtucket, Rhode Island, 2001.

[5] Leissa, A.W., "The Free Vibration of Rectangular Plates," *Journal of Sound and Vibration*, Vol. 31, No. 3, 1973, pp. 257-293.

[6] Waller, M., "Vibrations of Free Square Plates: Part I. Normal Vibrating Modes," *Journal of the Physical Society*, Vol. 51, No. 5, 1939, pp. 831-844.

[7] Blevins, R.D., **Formulas for Natural Frequency and Mode Shape**, Krieger Publishing Company, November 1993.

[8] Srinivas, S., Rao, A.K., "Bending, Vibration and Buckling of Simply Supported Thick Orthotropic Rectangular Plates and Laminates," *International Journal of Solids and Structures*, Vol. 6, 1970, pp. 1463-1481.

[9] Saltelli, A., Chan, K., Scott, M., Editors, **Sensitivity Analysis**, John Wiley & Sons, 2000.

[10] Myers, R.H., Montgomery, D.C., **Response Surface Methodology: Process and Product Optimization Using Designed Experiments**, Wiley Inter-science, New York, 1995.

[11] Kerschen, G., Golinval, J.C., Hemez, F.M., "Bayesian Model Screening for the Identification of Non-linear Mechanical Structures," *ASME Journal of Vibration and Acoustics*, Vol. 125, July 2003, pp. 389-397.

[12] Puel, G., Ladevèze, P., Romeuf, T., "How to Reduce the Lack of Knowledge of an Industrial Model in Structural Dynamics," *23rd SEM International Modal Analysis Conference*, Orlando, Florida, January 31-February 3, 2005.

[13] Hemez, F.M., Doebling, S.W., "Review and Assessment of Model Updating for Non-linear, Transient Dynamics," *Mechanical Systems and Signal Processing*, Special Issue "EuroMech-401, Inverse Methods in Structural Dynamics," Edited by J.E. Mottershead, Vol. 15, No. 1, January 2001, pp. 45-74.

[14] Booker, J.M., Ross, T.J., Rutherford, A.C., Reardon, B.J., Hemez, F.M., Anderson, M.C., Doebling, S.W., Joslyn, C.A., "An Engineering Perspective on Uncertainty Quantification for Validation, Reliability, and Certification," *Foundations'04 Workshop for Verification, Validation, and Accreditation in the 21st Century*, Arizona State University, Tempe, Arizona, October 13-15, 2004. Available as unlimited, public release LA-UR-04-6670 of the Los Alamos National Laboratory, Los Alamos, New Mexico.

[15] Hemez, F.M., "The Myth of Science-based Predictive Modeling," *Foundations'04 Workshop for Verification, Validation, and Accreditation in the 21st Century*, Arizona State University, Tempe, Arizona, October 13-15, 2004. Available as unlimited, public release LA-UR-04-6829 of the Los Alamos National Laboratory, Los Alamos, New Mexico.